Spectral interference effect in high-order harmonic generation with an ellipticity-modulated driving infrared pulse

Yinghui Zheng (郑颖辉), Hui Xiong (熊 辉), Zhinan Zeng (曾志男), Yiping Huo (霍义萍), Zhiguang Wang (王之光), Xiaochun Ge (葛晓春), Ruxin Li (李儒新), and Zhizhan Xu (徐至展)

Shanghai Institute of Optics and Fine Mechanics, Chinese Academy of Sciences, Shanghai 201800

A new physical explanation of the fringes in the high-order harmonic spectra generated by ellipticity-modulated infrared pulses is proposed, which is different from those in previous works. In this work we find that the fringes are due to the spectral interference effect induced by the two outgoing pulses with a delay, which are generated by the wave plates for ellipticity control. The visibility of interference fringes observed experimentally increases with the increase of the asymmetry of the two pulses, with the decrease of the delay and with the increase of peak intensity of the driving laser pulse. The experimental results are in good agreement with the calculated ones.

OCIS codes: 120.2650, 190.4160.

Coherent attosecond light pulses produced via high-order harmonic generation (HHG) bear the promise of probing inner-shell electronic motion in atoms with unprecedented resolution[1]. Due to the discrete nature and broad envelope spectrum of high-order harmonic emission, the appropriate phase locking of different harmonics can result in a train of pulses of attosecond duration[2−4].

The isolation of a single attosecond pulse from train remains a major physical challenge. The main problem to generate an isolated attosecond pulses is to confine the harmonic emission to less than one half optical cycle of the infrared (IR) pump laser pulse. The first method that achieved this goal requires phase stabilized, short enough (7 fs) laser pulses and a subsequent spectral filtering of cut off harmonics[5]. An alternative way to generate isolated XUV attosecond pulses is to rapidly modulate the polarization of the fundamental pulse and use the strong ellipticity dependence of HHG for confinement[6−11]. HHG efficiency is highest for linearly polarized driving laser fields and rapidly decreases with increasing driving ellipticity[12,13]. Therefore, under temporal modulation of the fundamental ellipticity, the harmonic emission is confined inside the temporal gate where the polarization is close to linear, as shown in recent experiments[14−16]. Different schemes have been proposed to generate ellipticity time-gate[11,14,17]. In 2004, such gate was obtained by superposing two few-cycle counter-circularly polarized pulses[18]. In the scheme, single attosecond pulses and XUV supercontinuum are produced in the high-order harmonic plateau. Also, a two-color pulse scheme is proposed by Huo *et al.*, which can produce single attosecond pulses with 20-fs laser pulses[19]. Recently, Sola *et al.* used two quartz plates in conjunction with carrier envelop phase (CEP) stabilized 5-fs pulses to create a polarization gate shorter than half of an optical cycle and obtain chirped isolated pulses of 205-as in experiment[20].

In these time-gate schemes, spectral interference fringes in the harmonic spectra generated by ellipticity-modulated IR pulses have ever been observed in experiment[9,14,15]. The phenomenon is considered as a red-shift in the harmonic spectra induced by the non-adiabatic effect in the harmonic generation process[9]. Altucci *et. al.* pointed out that it was due to the spectral splitting caused by the intrinsic harmonic chirp in the harmonic generation process[14]. In this work, the spectral interference fringes are also observed, where the high-order harmonic spectra are produced with an ellipticity-modulated driving IR pulse in a gas cell. This physical mechanism is analyzed experimentally and theoretically, which is different from those explanations in previous works. It is found that the interference effect is due to the two outgoing pulses with a delay after the two quartz wave plates used to generate ellipticity-modulated driving laser pulse. The interference visibility can be controlled by changing angles of the two wave plates, delays introduced by the wave plates, and intensity of the driving laser field. Furthermore, the measured harmonic spectra may be observed broadened due to the overlap of the interference fringes, so that the modulation of the harmonic spectral width in the time-gate schemes becomes difficult.

In our experiments, the driving laser field with a time-varying ellipticity is achieved with two quartz wave plates (one multiple-order $\lambda/4$ and one zero-order $\lambda/4$) as described in detail in Ref. [21]. The axis $O1$ of multiple-order quarter wave plate is at an angle α with respect to the initial direction of laser polarization and the axis $O2$ of zero-order quarter wave plate is at an angle β with respect to the direction of initial laser polarization. Tuning the angle between the respective neutral axes of the plates allows us to continuously vary the ellipticity of the laser field.

The initial fundamental field is assumed to be

$$E = 2E_0(t)\cos\left(\omega_0 t + \varphi - \frac{\pi}{4}\right), \tag{1}$$

where $E_0(t)$ is a slowly-varying envelope, ω_0 is the frequency and φ is the phase. For convenience, we project the field behind the two wave plates on the axes (x, y)

which are tuned by 45° with respect to the axes of the second wave plate ($o2, e2$):

$$E_x(t) = -2E_0^-(t)\cos\alpha\cos\frac{\pi}{4} \times\Bigg\{\cos(\alpha-\beta)\cos\left[\omega_0\left(t-\frac{\tau}{2}\right)+\varphi-\frac{\pi}{4}\right] +\sin(\alpha-\beta)\cos\left[\omega_0\left(t-\frac{\tau}{2}\right)+\varphi+\frac{\pi}{4}\right]\Bigg\} +2E_0^+(t)\sin\alpha\cos\frac{\pi}{4} \times\Bigg\{\sin(\alpha-\beta)\cos\left[\omega_0\left(t+\frac{\tau}{2}\right)+\varphi-\frac{\pi}{4}\right] -\cos(\alpha-\beta)\cos\left[\omega_0\left(t+\frac{\tau}{2}\right)+\varphi+\frac{\pi}{4}\right]\Bigg\}, \quad (2)$$

$$E_y(t) = -2E_0^-(t)\cos\alpha\sin\frac{\pi}{4} \times\Bigg\{\cos(\alpha-\beta)\cos\left[\omega_0\left(t-\frac{\tau}{2}\right)+\varphi-\frac{\pi}{4}\right] -\sin(\alpha-\beta)\cos\left[\omega_0\left(t-\frac{\tau}{2}\right)+\varphi+\frac{\pi}{4}\right]\Bigg\} +2E_0^+(t)\sin\alpha\sin\frac{\pi}{4} \times\Bigg\{\sin(\alpha-\beta)\cos\left[\omega_0\left(t+\frac{\tau}{2}\right)+\varphi-\frac{\pi}{4}\right] +\cos(\alpha-\beta)\cos\left[\omega_0\left(t+\frac{\tau}{2}\right)+\varphi+\frac{\pi}{4}\right]\Bigg\}, \quad (3)$$

$E_0^{\pm}(t) = E_0(t \pm \tau/2)$, and τ is the delay introduced by the multiple-order wave-plate between the orthogonal field components $E_0^+(t)$ and $E_0^-(t)$. We use the theoretical approach based on the current general quantum mechanical model by Lewenstein *et al.*[22] to calculate the XUV generation with arbitrary-polarized laser field.

We use a commercially available all-solid-state femtosecond laser system with 10-Hz repetition rate, 800-nm wavelength, 50-fs (full width at half maximum, FWHM) pulse duration and 25-mJ pulse energy. The energy after attenuation through a $\lambda/2$ wave plate and polarizing film is 8.5 mJ. The multi-order and zero-order $\lambda/4$ wave plates used to obtain a driving laser field with time-dependent polarization are placed after this attenuation part. Focused by a fused silica lens (focal length, $f = 815$ mm), the Gaussian laser beam fights its way through the stainless steel seals of the gas cell which are filled with argon. The high-order harmonics are emitted just in the gas cell. A flat-field X-ray spectrograph[23] is used to obtain the spectrum of high-order harmonics in the EUV and soft X-ray ranges. The spectrograph consists of a gold-coated spherical mirror, a gold-coated flat mirror, a slit, a Hitachi flat-field grating (1200 groove/mm), and a soft X-ray CCD (Princeton Instruments, 1340×400 imaging array PI-SX: 400). In the experiment, the intensity of the driving laser on the focus spot is $\sim 2\times10^{14}$ W/cm^2. The length of the cell is 11 mm.

For $\beta = 45°$, 135°, etc. (the so-called 'large gate configuration') as α is at 45°, the field produces a large temporal window for harmonic emission. On the contrary, for 90°, 180°, etc. (the so-called 'narrow gate configuration'), the field remains linearly polarized for a very short time[15]. Figure 1 presents experimental and calculated spectra of harmonics generated for large and narrow gates as α is at 45°. One can see the harmonics generated in the large gate exhibit interference fringe, as the two outgoing pulses after the two wave plates have a small delay. On the other hand, as the polarization gate becomes narrower, the delay increases and the two outgoing pulses part from each other, so no interference is observed in the harmonic spectra generated in the narrow gate. The interference fringes in the experimental spectra generated in the large gate overlap, thus the modulation depth of the fringes becomes small and the spectra are observed broadened. Nevertheless, although less pronounced, the interference fringe in the large gate is reproduced in the experimental spectra and a general agreement of the envelope of the spectra is observed.

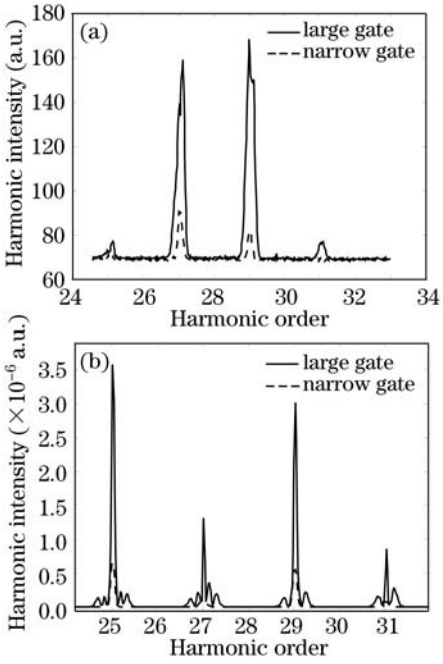

Fig. 1. (a) Measured and (b) calculated spectra generated for large gate (solid) and narrow gate (dash) as α is at 45°. Fundamental wavelength is 800 nm, peak intensity in the focus is $\sim 2\times10^{14}$ W/cm^2, initial pulse duration (after the wave plates) is $\tau_0 = 50$ fs and the delay induced by the multiple-order wave plate is $\tau = 46.1$ fs. Harmonics are generated in 11-mm-long gas cell target placed in the focus and filled with Ar of a backing pressure of 20.7 Torr.

Figure 2 shows the measured and calculated spectra generated for large and narrow gates as α is at 30° under the same conditions as in Fig. 1. One can see that the interference effect is more pronounced, the number of the fringe increases and two fringes are observed even in the spectra generated in the narrow gate. In order to clarify the formative mechanism of the fringe, in Fig. 3, we present calculated spectra generated for large and narrow gates as α is at 45°, 40°, 30° and 20° respectively. One can see that when the angle α changes from 45° to 30°, the interference pattern becomes more and more notable including the case in the narrow gate. When α is at 20°, the peak intensity of large gate field is much higher than

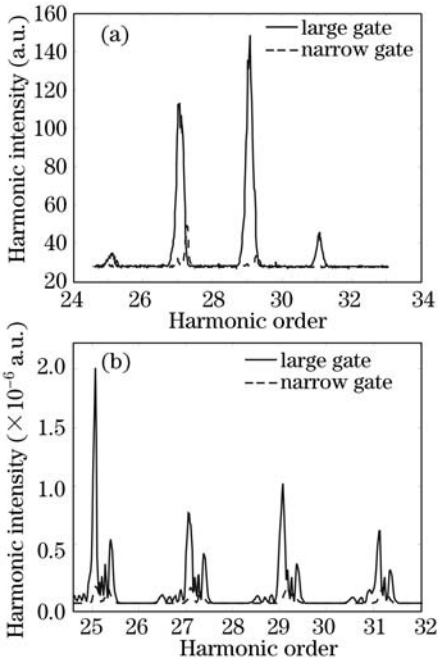

Fig. 2. (a) Measured and (b) calculated spectra generated for large gate (solid) and narrow gate (dash) as α is at 30° respectively under the same conditions as in Fig. 1.

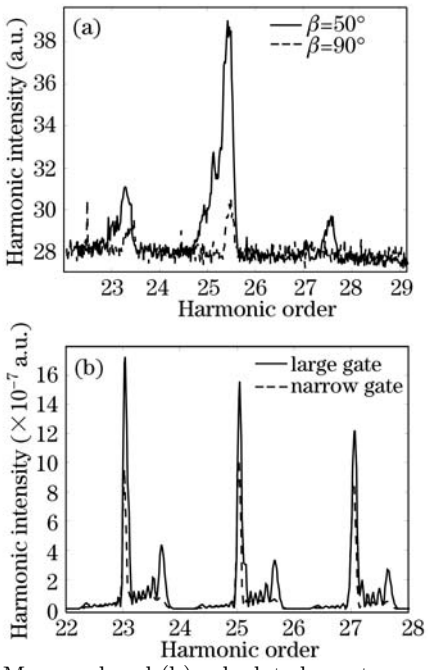

Fig. 4. (a) Measured and (b) calculated spectra generated for large gate (solid, $\beta = 50°$ in (a)) and narrow gate (dash) as α is at 45° respectively with the delay $\tau = 19.4$ fs.

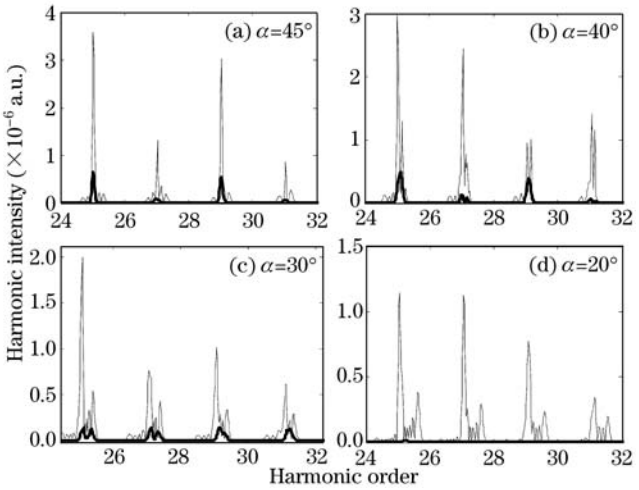

Fig. 3. Calculated spectra generated for large gate (thin line) and narrow gate (thick line) as α is at (a) 45°, (b) 40°, (c) 30° and (d) 20° under the same conditions as in Fig. 1.

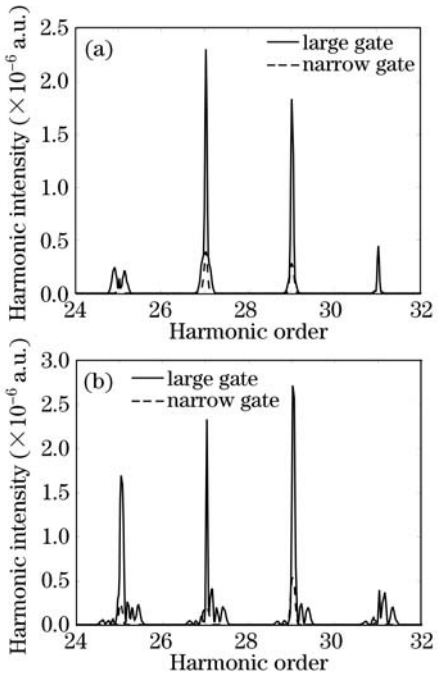

Fig. 5. Calculated spectra generated for large gate (solid) and narrow gate (dash) as α is at 45° with peak intensity of (a) 1.4×10^{14} and (b) 2.4×10^{14} W/cm^2 under the same conditions as in Fig. 1.

that of narrow gate field, so the interference continues to strengthen in the large gate while the harmonic spectra almost disappear in the narrow gate due to the weak intensity. It can be drawn from the above variable trend is that the interference effect due to the two outgoing pulses with a delay after the two wave plates and the asymmetry of the two pulses can enhance the interference pattern when the angle α is not set at 45°.

Figure 4 presents measured and calculated spectra generated for large and narrow gates as α is at 45° respectively, where the delay introduced by the multiple-order wave plate τ is 19.4 fs. Figure 5 shows calculated spectra generated for large and narrow gates as α is at 45° with peak intensity 1.4×10^{14} and 2.4×10^{14} W/cm^2, other conditions are the same as in Fig. 1. One can see that the interference effect induced by the two pulses generated through the two wave plates strengthens with the decrease of the delay and weakens with the decrease of peak intensity. To some extent, the asymmetry of the two pulses after the two wave plates is equivalent to the great decrease of the delay.

In this work, we investigate the physical mechanism of the spectra interference in the high-order harmonic spectra generated with an ellipticity-modulated driving IR pulse through a gas cell both experimentally and theoret-

ically. The conclusions we draw in this paper are different from the spectral red-shift explanation proposed before. We find that the interference effect is induced by the two outgoing pulses with a delay generated through the two wave plates. We can control the interference visibility by changing the angles of the two quartz wave plates, delays introduced by the wave plates, and intensity of the driving laser field. The interference effect strengthens with the increase of the asymmetry of the two pulses generated through the two wave plates, with the decrease of the delay, and with the increase of peak intensity. Furthermore, the measured harmonic spectra may be observed broadened due to the overlap of the interference fringes, so as to complicate significantly the modulation of the harmonic spectral width. From this point of view, it is necessary to eliminate the interference pattern from above three aspects.

Y. Zheng's e-mail address is yhzheng@siom.ac.cn.

References

1. M. Drescher, M. Hentschel, R. Kienberger, M. Uiberacker, V. Yakovlev, A. Scrinzi, T. Westerwalbesloh, U. Kleineberg, U. Heinzmann, and F. Krausz, Nature **419,** 803 (2002).
2. G. Farkas and C. Toth, Phys. Lett. A **168,** 447 (1992).
3. S. E. Harris, J. J. Macklin, and T. W. Hänsch, Opt. Commun. **100,** 487 (1993).
4. P. M. Paul, E. S. Toma, P. Breger, G. Mullot, F. Augé, Ph. Balcou, H. G. Muller, P. Agostini, Science **292,** 1689 (2001).
5. M. Hentschel, R. Kienberger, Ch. Spielmann, G. A. Reider, N. Milosevic, T. Brabec, P. Corkum, U. Heinzmann, M. Drescher, and F. Krausz, Nature **414,** 509 (2001).
6. P. B. Corkum, N. H. Burnett, and M. Y. Ivanov, Opt. Lett. **19,** 1870 (1994).
7. M. Ivanov, P. B. Corkum, T. Zuo, and A. Bandrauk, Phys. Rev. Lett. **74,** 2933 (1995).
8. Ph. Antoine, B. Piraux, D. B. Milosevic, and M. Gajda, Phys. Rev. A **54,** R1761 (1996).
9. V Strelkov, A Zair, O. Tcherbakoff, R. López-Martens, E. Cormier, E. Mével, and E. Constant, J. Phys. B **38,** L161 (2005).
10. V. T. Platonenko and V. V. Strelkov, J. Opt. Soc. Am. B **16,** 435 (1999).
11. M. Kovaŏev, Y. Mairesse, E. Priori, H. Merdji, O. Tcherbakoff, P. Monchicourt, P. Breger, E. Mével, E. Constant, P. Saliéres, B. Carré, and P. Agostini, Eur. Phys. J. D **26,** 79 (2003).
12. K. S. Budil, O. Salières, M. D. Perry, and A. L'Huillier, Phys. Rev. A **48,** R3437 (1993).
13. P. Dietrich, N. H. Burnett, M. Ivanov, and P. B. Corkum, Phys. Rev. A **50,** R3585 (1994).
14. C. Altucci, Ch. Delfin, L. Roos, M. B. Gaarde, A. L'Huillier, I. Mercer, T. Starczewski, and C.-G. Wahlström, Phys. Rev. A **58,** 3941 (1998).
15. O. Tcherbakoff, E. Mével, D. Descamps, J. Plumridge, and E. Constant, Phys. Rev. A **68,** 043804 (2003).
16. R. López-Martens, J. Mauritsson, P. Johnsson, and A. L'Huillier, Phys. Rev. A **69,** 053811 (2004).
17. N. A. Papadogiannis, G. Nersisyan, E. Goulielmakis, M. Decros, M. Tatarakis, E. Hertz, L. A. A. Nikolopoulos, D. Charalambidis, G. D. Tsakiris, P. Tzallas, and K. Witte, Proc. SPIE **5120,** 269 (2003).
18. Z. Chang, Phys. Rev. A **70,** 043802 (2004).
19. Y. Huo, Z. Zeng, R. Li, and Z. Xu, Opt. Express **13,** 9897 (2005).
20. I. J. Sola, Nature Physics **2,** 319 (2006).
21. V. Strelkov, A. Zair, O. Tcherbakoff, R. López-Martens, E. Cormier, E. Mével, and E. Constant, Appl. Phys. B **78,** 879 (2004).
22. M. Lewenstein, Ph. Balcou, M. Yu. Ivanov, A. L'Huillier, and P. B. Corkum, Phys. Rev. A **49,** 2117 (1994).
23. R. Li, P. Fan, Z. Xu, Z. Zhang, X. Feng, X. Wang, and P. Lu, J. Opt. (Paris) **25,** 143 (1994).